Dichotomous Well-defined Nanostructure with Weakly Arranged Ion Packing Explains the Solvency of Pyrrolidinium Acetate

Haihui Joy Jiang,[a] Silvia Imberti,[b] Rob Atkin,[c] and Gregory G. Warr*,[a]

[a]School of Chemistry and Australian Institute for Nanoscale Science and Technology, The University of Sydney, NSW 2006, Australia

[b]STFC, Rutherford Appleton Laboratory, Didcot, UK

[c]School of Molecular Sciences, The University of Western Australia, WA 6009, Australia

*E-mail: gregory.warr@sydney.edu.au

Abstract

Pyrrolidinium ionic liquids, especially pyrrolidinium acetate (PyrrAc), have demonstrated outstanding capacity for extracting lignin from biomass, as electrolytes for fuel cells and lithium ion batteries and as solvents for acid-catalysed reactions. In this work we show that the unusual liquid nanostructure of PyrrAc is the key to its versatility as a solvent compared to other ionic liquids. Neutron diffraction with multiple H/D isotopic substitutions reveals that the bulk nanostructure of PyrrAc is a bicontinuous network of interpenetrating polar and apolar domains. However, the arrangement of groups in both domains is strikingly different from that found in other ionic liquids. In the apolar regions, the pyrrolidinium rings are highly intercalated and disordered, with no preferred alignment between adjacent pyrrolidinium rings, which distinguishes it from both π–π stacking seen in imidazolium or pyridinium ionic liquids, and the tail-tail bilayer-like arrangements in linear alkylammonium ionic liquids. The H-bond network within the polar domain extends only to form finite clusters, with long bent H-bonds to

accommodate electrostatics. Therefore, while PyrrAc unquestionably has well defined amphiphilic nanostructure, the disordered arrangement of groups in the polar and apolar domains enables it to accommodate a wide variety of solutes. The combination of well-defined polar/apolar nanostructure, but disordered arrangements of groups within domains, is therefore the origin of PyrrAc's capacity for lignin extraction and as an electrolyte.

Introduction

Ionic liquids (ILs) are pure salts with low melting points. Composed entirely of ions, ILs possess a number of attractive and environmentally-friendly properties, including high thermal stability and negligible vapor pressure. Their excellent solubilizing capacity for solutes of different polarities[1, 2, 3, 4] has led to their adoption as designer solvents, where liquid properties are readily tunable by varying cation and anion structure.[5] From synthesis to catalysis, from electrochemistry to colloid science, ILs have repeatedly demonstrated performance advantages over molecular solvents.[6, 7, 8]

The liquid structures of a wide variety of aprotic ILs (typically comprising N-alkyl-substituted imidazolium, pyridinium, or quaternary ammonium cations) as well as protic ILs (PILs, often primary ammonium salts) with a range of anions have been investigated by x-ray and neutron diffraction, as well as by simulation techniques.[9, 10, 11, 12] These studies have highlighted the prevalence of amphiphilic nanostructure in ILs, with the liquid state frequently comprising charged, polar and uncharged, non-polar domains.[13, 14] This structural feature is thought to be a particularly significant determinant of the solvent properties of ILs for complex organic solutes.[15, 16, 17] Aprotic ILs have been more extensively studied, but PILs have the advantages of simpler synthesis and structure, and lower cost, which must be traded off against questions around exchangeable protons and ionicity.[18] Systematic studies have shown how amphiphilic nanostructure in PILs depends on cation and anion structure, and H-bond capacity.[19, 20] While electrostatic forces drive amphiphilic nanostructure, the H-bond network in PILs is correlated to several liquid properties.[21]

The majority of studies on aprotic ILs involve aromatic cations, with the archetype being N-methyl–N'-alkylimidazolium ($C_nC_1$im) salts. In these and similar aprotic ILs, the polar domains are comprised of the anion, the imidazolium ring and one or two adjacent methylenes on the alkyl chain that are polarized by the charged group. Nanostructure becomes increasingly prevalent as the alkyl chain length is increased beyond a propyl moiety; butyl or longer alkyl chains impart sufficient amphiphilicity to the cation sufficiently to drive segregation of non-polar domains. Such aprotic IL cations are highly reminiscent of conventional cationic surfactants, even to the extent that methylenes adjacent to the cation charge centre are often not regarded as truly non-polar.[22, 23, 24, 25] Further developing this analogy, Kashyap *et al*. have shown that liquid structure in a series of aprotic (and hence non-H-bonding) *N*-alkyl-*N*-methylpyrrolidinium bis(trifluoromethylsulfonyl)amide ILs is strongly affected by whether the cation alkyl tails are linear, branched or cyclic,[10] paralleling the self-assembly patterns of surfactants with different tail structures.[26, 27] In both cases the periodicity of the nanostructure is more sensitive to the length than it is to the volume of the alkyl chain.

PILs typically exhibit amphiphilic nanostructure on much shorter length scales than their aprotic counterparts. This is primarily due to the highly localized charge on primary ammonium cations, which allows polar/apolar segregation and amphiphilic nanostructure even in ethylammonium salts.[28, 29] The drawback of PILs for many applications arises from acid-base proton transfer, limiting the type of anions that can be employed while maintaining high ionicity and low vapour pressure.

Pyrrolidinium protic ionic liquids have recently been shown to have outstanding potential as solvents or electrolytes in a range of applications. Pyrrolidinium acetate (PyrrAc) shows particular promise for the extraction of lignin from lignocellulosic biomass when compared to

benchmark pyridinium and imidazolium systems.[30, 31] C_2C_1im acetate has been extensively studied for use in biorefineries with a variety of biomass types,[32, 33] suggesting PyrrAc would be an economically-attractive alternative. PyrrAc has also shown good potential as an acid-catalyzed reaction environment.[34] Several pyrrolidinium ILs have a wide electrochemical window compared to other PILs, making them suitable candidate electrolytes in capacitors, fuel cells, and lithium ion batteries.[34, 35, 36] In the context of this work, Margulis *et al*. have also shown the impact of ionic liquid nanostructure on the transport of both neutral and charged species.[37, 38, 39]

Here we seek to understand how the liquid structure of PyrrAc determines its performance in these diverse applications, and what design features are desirable for other ionic liquids. PyrrAc in many ways is a bridge between N-substituted pyridinium, imidazolium aprotic ILs and primary alkylammonium PILs, which retains the high synthetic atom efficiency of PILs and good potential for large scale uptake. Unlike pyrrolidinium nitrate, which is an energetic material,[40] the acetate is a stable and benign anion. As pyrrolidine is a stronger base than alkylamines, pyridine or imidazolium, pyrrolidinium (pK_a = 11.27) will be much less deprotonated by acetate than other protic cations.[41, 42] Thus, pyrrolidinium acetate is expected to have a high ionicity, and therefore have the potential to electrostatically drive polar/apolar segregation between the charge centres and ring carbons.

We determine the liquid structure of PyrrAc at high resolution by neutron diffraction. Results are analyzed by empirical potential structure refinement (EPSR), which simultaneously converges a Monte-Carlo simulation to diffraction patterns of multiple, isotopically-substituted (H/D) samples. To make a systematic comparison between PyrrAc to previously studied alkylammonium PILs, first we investigate how a secondary ammonium differs from primary

ammonium cations; As a secondary ammonium cation, pyrrolidinium has a lower capacity to form the dense, extended, three-dimensional, H-bond network that has been implicated in the structure and properties of other PILs,[21, 43, 44] and in amphiphilic nanostructure in general.[45, 46] Second, we explore how acetate differs from nitrate and formate anions. Lastly, we examine how the saturated pyrrolidinium ring affects liquid structure compared to both a primary ammonium chain and to an aromatic ring.

Experimental Section

Three chemically identical, but isotopically distinct PyrrAc samples were prepared: H-PyrrAc is fully hydrogenous, D4-PyrrAc is deuterated on the acetate methyl group and half the exchangeable protons on $Pyrr^+$, and D8-PyrrAc is deuterated on the cation ring. This selective deuteration method is known as contrast variation, which highlights molecular regions of interest in the neutron diffraction experiment.

PyrrAc samples were synthesized via acid-base neutralization from neat reagents in 1:1 mole ratio. H-PyrrAc was synthesized using pyrrolidine (Fluka, >99%) and acetic acid (VWR, >99.9%). D4-PyrrAc was synthesized from D4-acetic acid (Cambridge Isotopes, D99.5%) and hydrogenous pyrrolidne. D8-PyrrAc was synthesized from D8-pyrrolidine (Cambridge Isotopes, D98%) and hydrogenous acetic acid. All ILs were synthesized neat and reactions were maintained below 10˚C in an ice bath.Vacuum drying was avoided as the acid:base ratio changes under low pressure. Water contents were measured to be in between 0.4-0.6 wt% by Karl Fischer (Metrohm) volumetric titration. Over the period of a two-month experiment the maximum water content was 0.9wt%, which is equivalent to a water:ion ratio of 1:30. According to our structural

study of PIL-water mixture, such water content is unlikely to influence the present interpretation.[47] The amide content was monitored by ^{1}H-NMR 300MHz (Bruker) on regularly collected samples. Ionic liquid peaks were observed at 1.80-2.05 ppm (anions) and 3.15-3.35 ppm (cations), with D_2O as the solvent (δ_{solv} = 4.75 ppm). In the case of amide formation, we expect to see downfield shifts, observing peaks at 2.05-2.10 ppm and 3.30-3.60 ppm respectively. Exchangeable protons of PyrrAc were detected near 9.0-11.5 ppm. PyrrAc samples are stable at room temperature with negligible amide content (< 1.0 wt% after one month).

Neutron diffraction was performed on the SANDALS instrument at the ISIS research facility, Rutherford Appleton Laboratories, UK. The neutron wavelength range is 0.05 – 4.5 Å, and data were collected over the wave vector range 0.05 to 50 Å^{-1}. Samples were contained in chemically inert, null scattering $Ti_{0.68}Zr_{0.32}$ flat plate cells with internal dimensions of 1 × 35 × 35 mm, with a known atom density of 0.0541 atoms/Å^3, and sealed with PTFE O-rings. Diffraction patterns were collected for empty cells, direct beam and a 3 mm thick a vanadium standard for calibration and normalization. All samples were measured under vacuum at 298 K, maintained by a recirculating heater (Julabo FP50). The net run time for each sample was *ca*. 8 hours. Filled cells were re-weighed after the measurement to confirm that there was no loss of sample.

Data reduction was carried out using GUDRUN, described in the ATLAS manual.[48] Calibration, background subtraction and corrections for single atom scattering and hydrogen inelasticity were applied. Empirical Potential Structure Refinement (EPSR) was used to fit the normalized data.[49, 50] The structure of PyrrAc and atomic labels are shown in Figure 1. EPSR performs a Monte Carlo simulation governed by Lennard-Jones potentials and atom-centreed point charges listed in Table 1,[9, 51] as well as chemical and physical constraints such as molecular

structure and liquid density. The simulation box was composed of 460 pyrrolidinium cations and 460 acetate anions, 46 Å along each axis. Over 5000 snapshots were accumulated prior to analysis. The size of the box is sufficient to capture the maximum structural periodicity detected experimentally of 7 Å. Tests with 600 and 2000 ion pairs, respectively, were consistent with the results reported below.

Table 1. Lennard–Jones and Coulombic charge parameters used in the EPSR model. [a]parameters derived from ref. 31, [b]parameters taken from ref. 9

Atom	ε (kJ mol^{-1})	σ (Å)	q (e)
pyrrolidinium cation[a]			
N	0.711	3.25	-0.160
H_N	0.126	2.50	0.400
C_1	0.276	3.50	-0.160
C_2	0.276	3.50	0.060
H_1	0.126	2.50	0.200
H_2	0.126	2.50	0.080
acetate anion[b]			
C_O	0.500	3.50	0.700
O_C	0.655	3.17	-0.800
C_M	0.500	3.50	-0.280
H_M	0.200	2.50	0.060

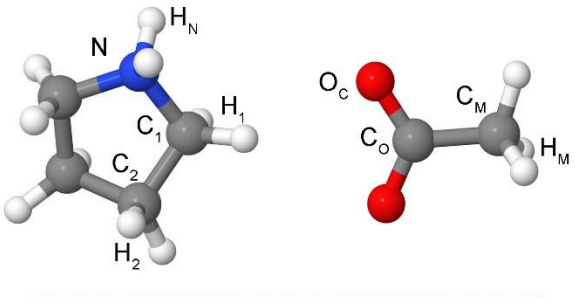

Figure 1. Structure and atomic labels for pyrrolidinium acetate (PyrrAc).

Results

Figure 2 shows the neutron diffraction data as structure factors, $S(q)$, for PyrrAc isotopomers in the range $0.0 < q < 18.0$ Å^{-1}. Varying the H/D isotopic composition creates three neutron contrasts: hydrogenous H-PyrrAc, d_4-PyrrAc with deuterated acetate and partially deuterated exchangeable amine protons, and d_8-PyrrAc with a deuterated cation ring. This distinguishes between protons with different hydrogen-bonding capacities. Simultaneous fitting to all contrasts shows good agreement between experimental data (dots) and EPSR calculation (solid lines). The slight disagreement at q = 2-3 Å^{-1} is an artifact, which exists in all three contrasts and did not change during the refinement process, therefore this did not influence final analysis. Scattering patterns at all contrasts have high q peaks > 1.5 Å^{-1}, corresponding to combinations of inter- or intra-ionic correlations.

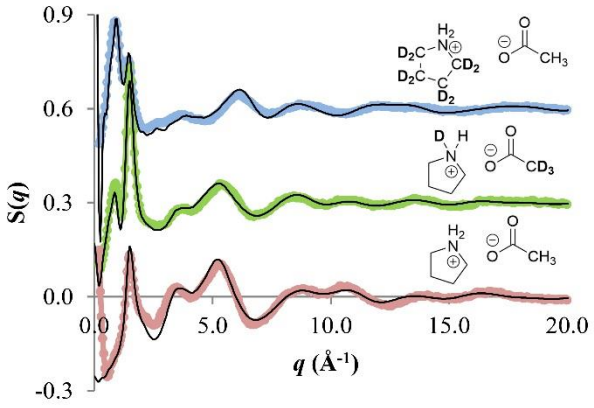

Figure 2. SANDALS experimental (coloured dots) and EPSR fitted (solid line) structure factors, S(q), as a function of wave vector, q, for three isotopomers of PyrrAc.

All three samples exhibit a pronounced Bragg peak at q = 1.5 Å^{-1}, corresponding to a nearest-neighbor (cation-anion) spacing of 4.2 Å (= $2\pi/q$). The other striking feature in Figure 2 is the presence of a peak at low q, visible in both partially-deuterated samples, d_8- and d_4-

PyrrAc. For both contrasts, this low-*q* peak lies at 0.90 $Å^{-1}$ corresponds to a periodicity of 7.0 Å, which is a combination of charge alternation and polar-apolar alternation.[52] Further analysis is required to distinguish among these correlations. In the case of an amphiphilic nanostructure, this repeat distance is smaller than the 10.0 - 10.2 Å periodic nanostructure seen in ethylammonium (EA^+) PILs.[13, 29]

Figure 3a shows representative snapshots of the simulation boxes captured after convergence to the experimental neutron diffraction results, with all atoms in standard atomic colors. Figure 3b shows the same snapshot, but with polar and apolar groups highlighted. This allows the visualization of how polar and apolar groups are distributed through the liquid. Apolar groups occupy a higher volume fraction than polar groups, and clearly form a continuous apolar domain. The distribution and connectivity of polar groups is less clear. Figures 3c shows snapshots through the simulation box of the locations of the polar ($>NH_2^+$ and $-CO_2^-$) and non-polar (C_4H_8 and $-CH_3$) groups; The extended connectivity of the non-polar groups is clear, but the polar domains are more isolated by comparison.

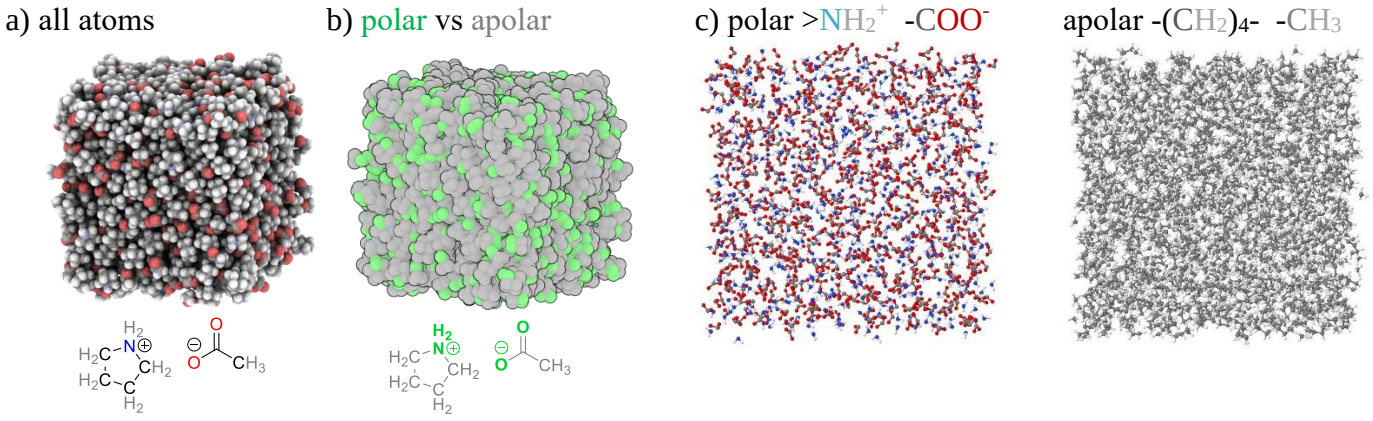

Figure 3. a) Representative snapshot of simulation box with 460 ion pairs converged to neutron diffraction patterns, in standard atomic colours; b) Snapshot derived from Figure 3a, with polar groups in green and apolar parts in grey; c) shows separately the polar and non-polar moieties, respectively, of both the cations and anions.

In order to look at atomic details in the polar region, Figure 4a shows partial pair correlation functions, $g_{ij}(r)$, between the H-bond donor and acceptor (H_N-O_C) and the corresponding charged centres (N-C_O) on the cation and anion. $g_{ij}(r)$ describe the radially-averaged distance-dependence of atom-atom correlations, obtained from the converged EPSR simulation. A complete set of $g_{ij}(r)$ is provided in SI. A peak in $g_{ij}(r)$ corresponds to a preferred correlation distance between atoms *i* and *j* and is strongest for nearest-neighbour correlations between cation-anion charged groups at short distances. The sharp peak at 2.38 Å in the ammonium H and anion O pair (H_N-O_C) correlation function represents the most probable H-bond distance. Between oppositely charged centres (N-C_O) there is also a peak, meaning that there is a strong cation-anion correlation due to Coulombic interactions.

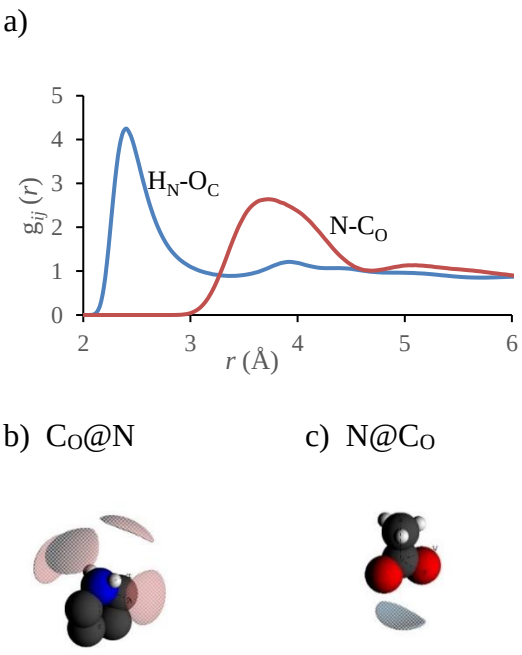

Figure 4. a) $g_{ij}(r)$ functions of PyrrAc in the polar region. Spatial distribution function (SDF) plots showing 20% probability surfaces for b) anion carboxyl carbon around cation ammonium, and c) cation ammonium around anion carboxyl.

The anisotropy of nearest-neighbour distributions between charged groups are shown in Figure 4b in the form of spatial distribution function (SDF). Lobes represent the most-probable arrangements of nearest-neighbours up to maximum radial distances corresponding to the first minimum in the corresponding $g_{ij}(r)$. Figure 4b (C_O@N) shows that the centre of the acetate carboxyl group is preferentially found in well-defined orientations around the ammonium group away from the saturated ring. There are two different types of preferred site, and each has two symmetry-equivalent lobes: in one the carboxyl group sits opposite the pyrrolidinium ring, but on either side of the ammonium centre. In the other the carboxyl sits to the side of ammonium at possible H-bonding sites. The complementary cation@anion (N@C_O) distribution, Figure 4c, shows a single preferred arrangement for the ammonium group that is highly localized between two acetate oxygens, opposite the acetate methyl. This spatial arrangement of ammonium around the carboxylic group is similar to that seen previously in a formate PIL, except that probability lobe is smaller here,[29] and is similar to the three lobe structure seen for ammonium charge centres around the more symmetric nitrate anion.[13]

Figure 5a shows the cation-anion hydrogen bond angle distribution in PyrrAc, compared to primary ammonium PILs including ethylammonium formate (EAF), ethyammonium nitrate (EAN) and propylammonium nitrate (PAN).[21] These PILs all show a broad distribution of angles, with the majority lying in between 90-170˚. This means that H-bonds in these ILs are mostly bent. Figure 5b shows the hydrogen bonds in PyrrAc separated by type based on the spatial distribution of atoms as 25.6% single, 14.4% bidentate, 27.2% bifurcated, 0.1% bridged and 32.7% multi-contact interactions. Also shown are bond-length/bond-angle distribution maps for the three main types, the majority of which are within the range of 2.2-2.8 Å and 110-170˚. As H_N-O_C distance increases, there is a shift towards lower bond angles for all H-bond types. Not

even the single H-bonds are predominantly linear at and bond length. The distribution of bifurcated H-bonds clearly lies at lower bond angles for a given bond length than either single or bidentate bonds. Note, however, that these classifications are based solely on N, H_N and O_C positions in the converged simulations and not on any energetic measure. The distribution of bidentate H-bonds thus includes a population of single H-bonds in which distal O_Cs have simply rotated near to H_N.

a)

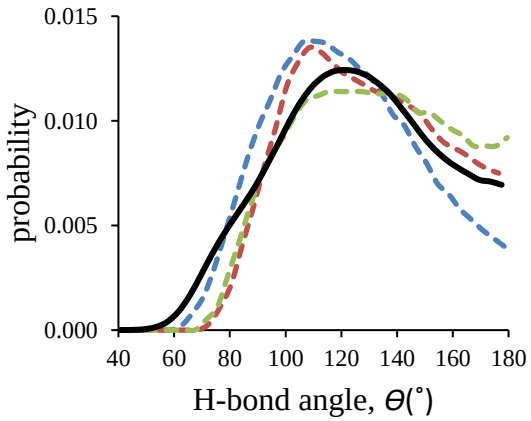

b)

Single 25.6%

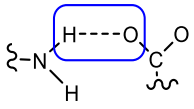

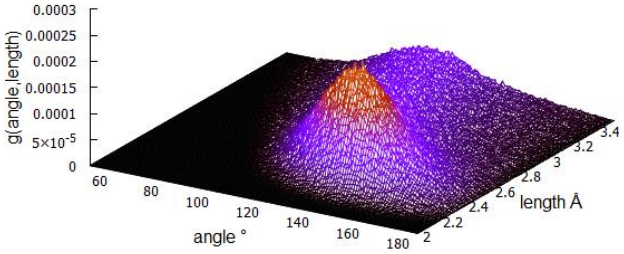

Bidentate 14.4%

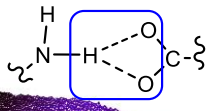

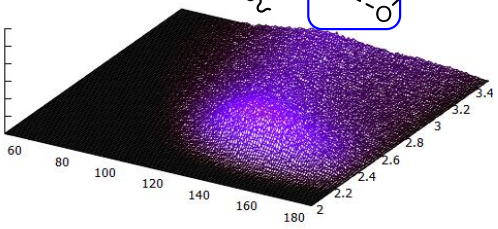

Bifurcated 27.2%

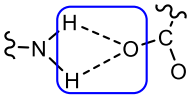

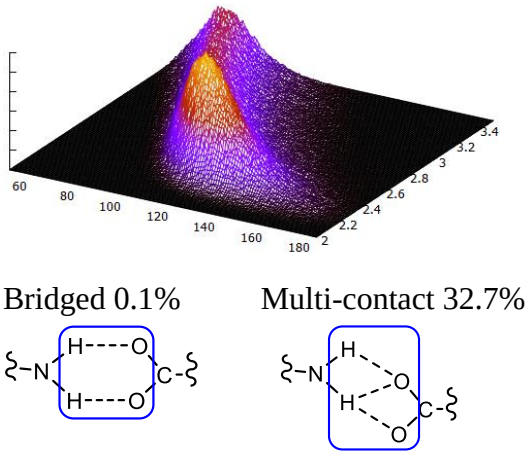

Figure 5. a) Hydrogen bond angle distribution of N-H_N···O_C (black), defined by bond lengths (H_N···O_C < 3.4 Å), compared to EAF (blue), EAN (red) and PAN (green).[21] b) Hydrogen bond angle-distance distribution maps with classification labelled.

These results highlight that the ionic arrangements in PyrrAc are dominated by electrostatic attractions between charges on the ammonium cation and carboxylate anion. Instead of forming a linear H-bonding network, the bond angle is distorted to accommodate closer approach of opposite charges.

Table 2 compares key hydrogen bond characteristics of the current and our previous studies on PILs, including PyrrAc, EAF, EAN and PAN. There also the local ion arrangements and H-bond network structure were found to be a consequence of the balance between Coulombic forces that drive polar-apolar nanosegregation, and the packing geometry of ions.[21] A different donor-acceptor ratio in PyrrAc means variations in geometric arrangement. Although all four ILs have long and bent H-bond, the coordination number of anion around cation varies significantly. Despite the structural similarity between acetate and formate anions, the H-bond geometry in PyrrAc is more similar to PAN than EAF.

Table 2. Average H-bond properties of protic ionic liquids. Data for ethylammonium formate (EAF), ethylammonium nitrate (EAN) and propylammonium nitrate (PAN) were extracted from previous work.[21]

	donor: acceptor	Length (Å)	Angle (˚)	Coord # (range Å)	Type
PyrrAc	2:2	2.43	120	1.8 (0-3.25)	Single/bifurcated
EAF	3:2	2.45	110	2.7 (0-3.25)	Bi/trifurcated
EAN	3:3	2.41	107	1.6 (0-3.00)	Bifurcated
PAN	3:3	2.37	117(broad)	2.1 (0-3.00)	Bifurcated

In order to quantitatively assess the microsegregation among polar groups in ionic liquid, cluster analysis was used over thousands iterations of the converged simulation box to calculate the fraction of ions, $f(n)$, in a cluster of size n. The results are shown in Figure 6. We perform three series of analysis on the same PyrrAc system: The first series (green) shows the distribution of "standard" H-bonds, defined by a distance between a H-donor (H_N) and a H-acceptor (O_C) less than 2.8 Å and bond angles between 90° and 180° (cf. Figure 5). The green series lies slightly above the predicted random 3-dimentional percolation threshold, derived from the probability function[53] (shown as a solid line), meaning that standard hydrogen bonds form a network that lies on the percolation threshold.

If we expand the definition to incorporate "distorted" H-bonds (up to 3.4Å, and angles from 60-180˚, shown in orange), then the fraction of small clusters (n < 30) decreases markedly and falls well below the percolation threshold. This decrease is offset by a population of large clusters on the right-hand side lying above the percolation threshold, which represents a continuous (simulation box spanning) network of polar groups that are not all connected by standard H-bonds.

This interpretation is substantiated by a cluster analysis of the electrostatic network, defined by a correlation distance between cation (N) and anion (C_O) charge centres, shown in blue. Here the nearest-neighbour cutoff distance is determined from the first minimum in the N-C_O $g_{ij}(r)$ (Figure 4a). The cluster distribution parallels that of the expanded H-bond series, and also produces a peak on the right-hand side. This means electrostatic interactions alone form a continuous network, with more than 99% of ions forming part of a single large cluster that lies far above the percolation threshold. This suggests that PyrrAc has a continuous polar domain with alternating charges, and it is primarily Coulombic in its origin. The hydrogen bond network within the polar domain is not continuous.

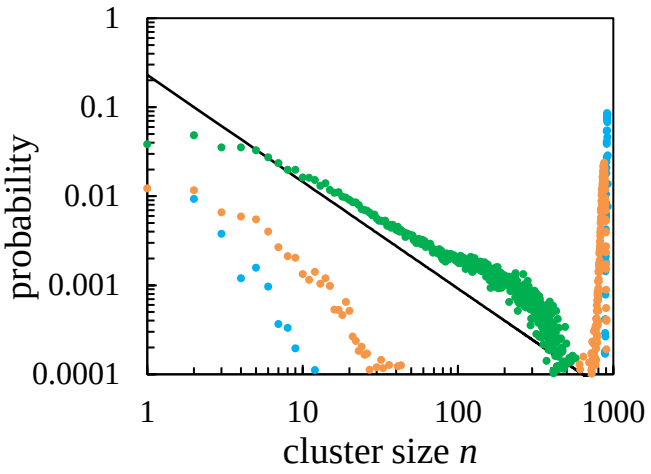

Series	Correlation	Length (Å)	H-bond Angle (˚)
Standard H-bond	$H_N - O_C$	0 - 2.8	90 - 180
Standard & distorted H-bond	$H_N - O_C$	0 - 3.4	60 - 180
Electrostatic	$N - C_O$	0 - 4.7	-

Figure 6. Cluster analysis of polar groups in PyrrAc, where probability $f(n)$ is the fraction of ions in a cluster of size n defined by nearest-neighbour distances and bond angles between different atom types derived from partial pair-correlation functions, $g_{ij}(r)$ (see text); black line is the theoretical percolation threshold $f(n) = n^{-1.2}/4.34$, see reference [53].

Knowing the structure in the polar region, we further look into interactions in the apolar region. Figure 7a shows key atomic partial pair correlation functions, $g_{ij}(r)$, among hydrocarbons. The $g_{ij}(r)$ function between acetate methyl carbons (C_M-C_M) has a peak near 4 Å, which is more pronounced than between terminal carbons of $Pyrr^+$ (C_2-C_2). This suggests stronger apolar-apolar correlation among the anions than among the cations. Acetate methyl groups are also correlated with a cation ring carbon (C_M-C_2), producing a peak with equal intensity to C_M-C_M. This suggests mixed association rather than the formation of distinct apolar regions of cation and anion.

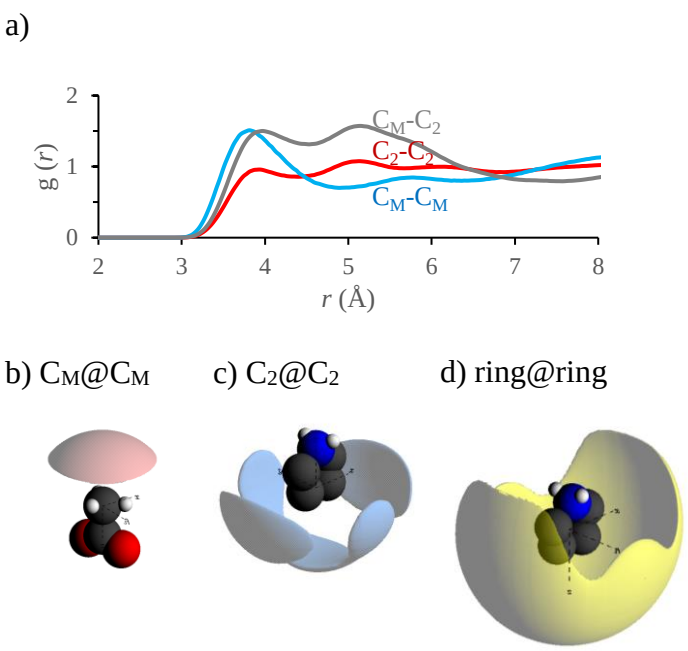

Figure 7. a) $g_{ij}(r)$ functions of selected hydrophobic groups of PyrrAc, showing correlation strength at a given distance. Also shown are spatial distribution function (SDF) plots showing 20% probability surfaces among b) anion methyl groups c) C_2 (bottom) carbons of the cation ring d) the cation ring geometric centers

Spatial distribution plots of apolar groups further support these conclusions. As shown in Figure 7b, there is a conventional 'tail-tail' arrangment of acetate ions. The acetate methyl group seems to induce an amphiphilic character in the anion not seen previously in structurally similar formate PILs; Extrapolating this trend, we would expect much stronger anion-induced nanostructure with longer alkanoate ILs.[54, 55] Although adding an extra level of complexity to the interactions, we note that this kind of anion association has also been reported previously for ILs with analogous fluorous anions, which in this case did yield separate hydrocarbon and fluorocarbon regions.[56, 57]

Association between cation ring carbons are shown through the $C_2@C_2$ distribution in Figure 7c. Although these probability lobes are not quite isotropic and exhibit some preferred orientations, they surround the sides and at the bottom of the cation ring and do not extend around the ammonium head group. This strong, amphiphilic association between pyrrolidinium rings is underscored by Figure 7d, which shows the spatial distribution of the geometric centres of cation rings. The most probable position of finding a second ring from a reference ring is around the carbon side of the cation (i.e. the relatively apolar region), and far away from the charged ammonium group. The ring-centre spatial distribution is essentially the complement of the anion spatial distribution (Figure 4b) around the cation charge.

This suggests that, although there is an association between nonpolar rings, there is no preferred specific arrangement for adjacent cation rings in PyrrAc, such as stacking. Figure 8 confirms that cation rings in PyrrAc do not adopt any preferred arrangement at any correlation distance by showing the angular radial distribution function, $g(r,\theta)$, where θ is the angle between the normals to each ring. The distribution is relatively flat with only small oscillations across all angles at short distances, and confirms that there is no strong preference towards any specific

alignment between adjacent rings. 2D projections supporting this conclusion, and which also validate the radius ranges used for the spatial probability distributions, are shown in SI.

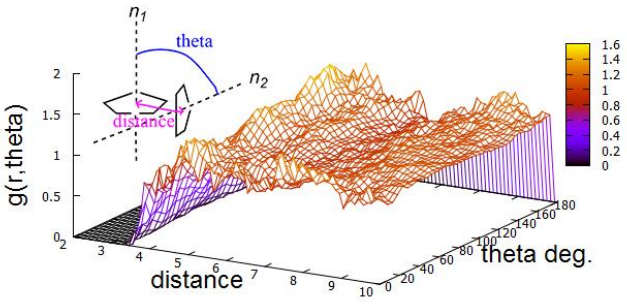

Figure 8. Angular radial distribution function plot for pyrrolidinium ring-centre—ring-centre, $g(r,\theta)$, where r is the distance (Å) between the centre of two rings and θ is the angle between the normal for cation ring-approximated planes shown on right. Analysis was performed using DLPUTILS.[58]

For aromatic liquids like benzene or pyridinium- and imidazolium-based aprotic ILs, π-π stacking is an important intermolecular interaction that can give rise to parallel and T-shaped orientations of neighbouring aromatic rings.[59, 60] However with saturated pyrrolidinium cations there are no such strong intermolecular interactions between rings, and steric effects are insufficient to induce any preferred arrangements.

Discussion and Conclusions

The liquid structure of PyrrAc qualitatively recapitulates the amphiphilic nanostructure seen in primary alkylammonium PILs, but highlights some important distinctive features. Cluster analysis has revealed that strong, Coulombic interactions between charged groups drive the segregation of uncharged groups and leads to the formation of a bicontinuous, system-spanning network of interpenetrating polar and non-polar domains. Within the polar domains, the H-bond

network is limited to a distribution of finite clusters within the extended polar domain. The H-bonds themselves are predominantly long and bent, accommodating electrostatics. Amphiphilic nanostructure remains a feature of this PIL, even though the density of H-bond donors and acceptors in the secondary ammonium cation and acetate anion is lower than in previously-studied systems.

The key difference between PyrrAc and previously-studied primary alkylammonium PILs is packing in the apolar region. $Pyrr^+$ cation rings are less ordered within the apolar domains that their praimary alkylammonium counterparts; Figure 7b highlights the lack of strong end-to-end correlations between ring C_2 carbons,[13, 19, 61] showing instead a high degree of ring intercalation. PyrrAc thus forms apolar domains that are thinner than the combined length of two cation rings, giving rise to the smaller observed periodic spacing for PyrrAc (7.0 Å) in comparison to EAN (10.0 Å) in their neutron diffraction patterns. Unlike nitrate or formate, the acetate methyl group clearly contributes to the amphiphilic nanostructure of PyrrAc.

The relative sizes of the polar and nonpolar part of an IL define a packing geometry (a_{alkyl}/a_{polar}), similar to the packing parameter used for surfactants.[62, 63] Linear PILs of similar molecular lengths, such as ethylammonium nitrate and formate, have packing parameters of $a_{alkyl}/a_{polar} \sim 1$, forming a bicontinuous sponge-like structure, built up from a locally *bilayer-like* arrangement of cations oriented tail-tail with their terminal methyls opposite each other, and a mean curvature of the polar/apolar interface near zero.[29] The larger non-polar volume in PyrrAc at near-constant alkyl length and polar group size, yielding $a_{alkyl}/a_{polar}. > 1$, gives rise to an inverted structure, analogous to a bicontinuous microemulsion near its transition to discrete water-in-oil droplets.[26, 64, 65]

Phenolic compounds, such as lignin decomposition products, are challenging solutes because they consist of small polar and apolar domains. Many other ionic liquids have bicontinuous nanostructure,[12] but with ordered polar and apolar domains that become more ordered as the cation is made more amphiphilic.[9, 61] These well-defined ion arrangements do not easily adjust to incorporate solutes of closely associated polar and hydrophobic groups, resulting in a high energetic cost. PyrrAc, on the other hand, has well defined nanostructure but the arrangements of groups within the polar and apolar domains are flexible, and therefore can readily adapt to the structure of phenolic compounds with minimal energetic cost; i.e. with less disruption to their existing disordered structure.[66, 67] Likewise, the distorted and adaptable H-bond network of PyrrAc facilitates the dissolution and solvation of other polar groups including lithium and other ions.[36]

Supporting Information

S1. Additional Partial Pair Correlation Functions

S2. 2D Map of the Ring-Ring Distribution

Acknowledgments

HJJ thanks the University of Sydney for a Henrie Bertie and Florence Mabel Gritton Research Scholarship and AINSE for an Honours Scholarship. RA thanks the ARC for a Future Fellowship. This research was supported by an ARC Discovery Project and an ISIS beamtime grant. The authors thank Tristan Youngs for developing DLPUTILS (for simulation analysis) and Tom Headen from ISIS and Blake Simmons of the US Department of Energy's Joint BioEnergy Institute for valuable discussions.

References

1. Earle, M. J.; Esperanca, J. M.; Gilea, M. A.; Lopes, J. N.; Rebelo, L. P.; Magee, J. W.; Seddon, K. R.; Widegren, J. A. The Distillation and Volatility of Ionic Liquids. *Nature* **2006,** *439*, 831-834.
2. MacFarlane, D. R.; Seddon, K. R. Ionic Liquids - Progress on the Fundamental Issues. *Aust. J. Chem.* **2007,** *60*, 3-5.
3. Earle, M. J.; Seddon, K. R. Ionic Liquids: Green Solvents for The Future. *Pure Appl. Chem.* **2000,** *72*, 1391-1398.
4. Angell, C. A.; Byrne, N.; Belieres, J. P. Parallel Developments in Aprotic and Protic Ionic Liquids: Physical Chemistry and Applications. *Acc. Chem. Res.* **2007,** *40*, 1228-1236.
5. Hayes, R.; Warr, G. G.; Atkin, R. At the Interface: Solvation and Designing Ionic Liquids. *Phys. Chem. Chem. Phys.* **2010,** *12*, 1709-1723.
6. Endres, F. Ionic Liquids: Solvents for the Electrodeposition of Metals and Semiconductors. *ChemPhysChem* **2002,** *3*, 145-154.
7. Welton, T. Room-Temperature Ionic Liquids. Solvents for Synthesis and Catalysis. *Chem. Rev.* **1999,** *99*, 2071-2084.
8. Antonietti, M.; Kuang, D.; Smarsly, B.; Zhou, Y. Ionic Liquids for the Convenient Synthesis Of Functional Nanoparticles and Other Inorganic Nanostructures. *Angew. Chem., Int. Ed.* **2004,** *43*, 4988-4992.
9. Bowron, D. T.; D'Agostino, C.; Gladden, L. F.; Hardacre, C.; Holbrey, J. D.; Lagunas, M. C.; McGregor, J.; Mantle, M. D.; Mullan, C. L.; Youngs, T. G. Structure and Dynamics of 1-Ethyl-3-Methylimidazolium Acetate via Molecular Dynamics and Neutron Diffraction. *J. Phys. Chem. B* **2010,** *114*, 7760-7768.
10. Kashyap, H. K.; Santos, C. S.; Murthy, N. S.; Hettige, J. J.; Kerr, K.; Ramati, S.; Gwon, J.; Gohdo, M.; Lall-Ramnarine, S. I.; Wishart, J. F., et al. Structure of 1-Alkyl-1-Methylpyrrolidinium Bis(Trifluoromethylsulfonyl)Amide Ionic Liquids with Linear, Branched, and Cyclic Alkyl Groups. *J. Phys. Chem. B* **2013,** *117*, 15328-15337.
11. Murphy, T.; Atkin, R.; Warr, G. G. Scattering from Ionic Liquids. *Curr. Opin. Colloid Interface Sci.* **2015,** *20*, 282-292.
12. Hayes, R.; Warr, G. G.; Atkin, R. Structure and Nanostructure in Ionic Liquids. *Chem. Rev.* **2015,** *115*, 6357-426.
13. Hayes, R.; Imberti, S.; Warr, G. G.; Atkin, R. Amphiphilicity Determines Nanostructure in Protic Ionic Liquids. *Phys. Chem. Chem. Phys.* **2011,** *13*, 3237-3247.
14. Triolo, A.; Russina, O.; Bleif, H. J.; Di Cola, E. Nanoscale Segregation in Room Temperature Ionic Liquids. *J. Phys. Chem. B* **2007,** *111*, 4641-4644.
15. Topolnicki, I. L.; FitzGerald, P. A.; Atkin, R.; Warr, G. G. Effect of Protic Ionic Liquid and Surfactant Structure on Partitioning Of Polyoxyethylene Non-Ionic Surfactants. *ChemPhysChem* **2014,** *15*, 2485-2489.
16. Greaves, T. L.; Drummond, C. J. Solvent Nanostructure, the Solvophobic Effect and Amphiphile Self-Assembly in Ionic Liquids. *Chem. Soc. Rev.* **2013,** *42*, 1096-1120.
17. Hao, J. C.; Zemb, T. Self-Assembled Structures and Chemical Reactions In Room-Temperature Ionic Liquids. *Curr. Opin. Colloid Interface Sci.* **2007,** *12*, 129-137.
18. George, A.; Brandt, A.; Tran, K.; Zahari, S. M. S. N. S.; Klein-Marcuschamer, D.; Sun, N.; Sathitsuksanoh, N.; Shi, J.; Stavila, V.; Parthasarathi, R., et al. Design of Low-Cost Ionic Liquids for Lignocellulosic Biomass Pretreatment. *Green Chem.* **2015,** *17*, 1728-1734.
19. Hayes, R.; Imberti, S.; Warr, G. G.; Atkin, R. Pronounced Sponge-Like Nanostructure in Propylammonium Nitrate. *Phys. Chem. Chem. Phys.* **2011,** *13*, 13544-13551.

20. Greaves, T. L.; Kennedy, D. F.; Mudie, S. T.; Drummond, C. J. Diversity Observed in the Nanostructure of Protic Ionic Liquids. *J. Phys. Chem. B* **2010,** *114*, 10022-10031.
21. Hayes, R.; Imberti, S.; Warr, G. G.; Atkin, R. The Nature of Hydrogen Bonding in Protic Ionic Liquids. *Angew. Chem., Int. Ed.* **2013,** *52*, 4623-4627.
22. Nagarajan, R. Solubilization in Aqueous Solutions of Amphiphiles. *Curr. Opin. Colloid Interface Sci.* **1996,** *1*, 391-401.
23. Zana, R. Aqueous Surfactant-Alcohol Systems - a Review. *Adv. Colloid Interface Sci.* **1995,** *57*, 1-64.
24. Aamodt, M.; Landgren, M.; Jonsson, B. Solubilization of Uncharged Molecules in Ionic Surfactant Aggregates 1. The Micellar Phase. *J. Phys. Chem.* **1992,** *96*, 945-950.
25. Almgren, M.; Grieser, F.; Thomas, J. K. Dynamic and Static Aspects of Solubilization of Neutral Arenes in Ionic Micellar Solutions. *J. Am. Chem. Soc.* **1979,** *101*, 279-291.
26. Chen, V.; Warr, G. G.; Evans, D. F.; Prendergast, F. G. Curvature and Geometric Constraints as Determinants of Microemulsion Structure - Evidence from Fluorescence Anisotropy Measurements. *J. Phys. Chem.* **1988,** *92*, 768-773.
27. Nave, S.; Eastoe, J.; Heenan, R. K.; Steytler, D.; Grillo, I. What is so Special about Aerosol-OT? 2. Microemulsion Systems. *Langmuir* **2000,** *16*, 8741-8748.
28. Atkin, R.; Warr, G. G. The Smallest Amphiphiles: Nanostructure in Protic Room-Temperature Ionic Liquids with Short Alkyl Groups. *J. Phys. Chem. B* **2008,** *112*, 4164-4166.
29. Hayes, R.; Imberti, S.; Warr, G. G.; Atkin, R. Effect of Cation Alkyl Chain Length and Anion Type on Protic Ionic Liquid Nanostructure. *J. Phys. Chem. C* **2014,** *118*, 13998-14008.
30. Achinivu, E. C.; Howard, R. M.; Li, G. Q.; Gracz, H.; Henderson, W. A. Lignin Extraction from Biomass with Protic Ionic Liquids. *Green Chem.* **2014,** *16*, 1114-1119.
31. George, A.; Tran, K.; Morgan, T. J.; Benke, P. I.; Berrueco, C.; Lorente, E.; Wu, B. C.; Keasling, J. D.; Simmons, B. A.; Holmes, B. M. The Effect of Ionic Liquid Cation and Anion Combinations on the Macromolecular Structure of Lignins. *Green Chem.* **2011,** *13*, 3375-3385.
32. Shi, J.; Thompson, V. S.; Yancey, N. A.; Stavila, V.; Simmons, B. A.; Singh, S. Impact of Mixed Feedstocks and Feedstock Densification on Ionic Liquid Pretreatment Efficiency. *Biofuels* **2013,** *4*, 63-72.
33. Çetinkol, Ö. P.; Dibble, D. C.; Cheng, G.; Kent, M. S.; Knierim, B.; Auer, M.; Wemmer, D. E.; Pelton, J. G.; Melnichenko, Y. B.; Ralph, J., et al. Understanding the Impact of Ionic Liquid Pretreatment on Eucalyptus. *Biofuels* **2010,** *1*, 33-46.
34. Anouti, M.; Caillon-Caravanier, M.; Dridi, Y.; Galiano, H.; Lemordant, D. Synthesis and Characterization of New Pyrrolidinium Based Protic Ionic Liquids. Good and Superionic Liquids. *J. Phys. Chem. B* **2008,** *112*, 13335-13343.
35. Anouti, M.; Timperman, L. A Pyrrolidinium Nitrate Protic Ionic Liquid-Based Electrolyte for Very Low-Temperature Electrical Double-Layer Capacitors. *Phys. Chem. Chem. Phys.* **2013,** *15*, 6539-6548.
36. Vogl, T.; Menne, S.; Kuhnel, R. S.; Balducci, A. The Beneficial Effect of Protic Ionic Liquids on the Lithium Environment in Electrolytes for Battery Applications. *J. Mater. Chem. A* **2014,** *2*, 8258-8265.
37. Araque, J. C.; Yadav, S. K.; Shadeck, M.; Maroncelli, M.; Margulis, C. J. How is Diffusion of Neutral and Charged Tracers Related to the Structure and Dynamics of a Room-Temperature Ionic Liquid? Large Deviations from Stokes–Einstein Behavior Explained. *J. Phys. Chem. B* **2015,** *119*, 7015-7029.
38. Araque, J. C.; Hettige, J. J.; Margulis, C. J. Modern Room Temperature Ionic Liquids, a Simple Guide to Understanding Their Structure and How It May Relate to Dynamics. *J. Phys. Chem. B* **2015,** *119*, 12727-12740.
39. Kashyap, H. K.; Annapureddy, H. V. R.; Raineri, F. O.; Margulis, C. J. How is Charge Transport Different in Ionic Liquids and Electrolyte Solutions? *J. Phys. Chem. B* **2011,** *115*, 13212-13221.
40. Wellens, S.; Thijs, B.; Binnemans, K. How Safe are Protic Ionic Liquids? Explosion of Pyrrolidinium Nitrate. *Green Chem.* **2013,** *15*, 3484-3485.

41. Hall, H. K. Correlation of the Base Strengths of Amines. *J. Am. Chem. Soc.* **1957,** *79*, 5441-5444.
42. Walba, H.; Isensee, R. W. Acidity Constants of Some Arylimidazoles and Their Cations. *J. Org. Chem.* **1961,** *26*, 2789-2791.
43. Evans, D. F.; Chen, S.; Schriver, G. W.; Arnett, E. M. Thermodynamics of Solution of Nonpolar Gases in a Fused Salt. Hydrophobic Bonding Behavior In A Nonaqueous System. *J. Am. Chem. Soc.* **1981,** *103*, 481-482.
44. Greaves, T. L.; Drummond, C. J. Solvent Nanostructure, the Solvophobic Effect and Amphiphile Self-Assembly in Ionic Liquids. *Chem.Soc.Rev.* **2013,** *42*, 1096-1120.
45. Ray, A. Solvophobic Interactions and Micelle Formation in Structure Forming Nonaqueous Solvents. *Nature* **1971,** *231*, 313-315.
46. Greaves, T. L.; Kennedy, D. F.; Weerawardena, A.; Tse, N. M. K.; Kirby, N.; Drummond, C. J. Nanostructured Protic Ionic Liquids Retain Nanoscale Features in Aqueous Solution while Precursor Bronsted Acids and Bases Exhibit Different Behavior. *J. Phys. Chem. B* **2011,** *115*, 2055-2066.
47. Hayes, R.; Imberti, S.; Warr, G. G.; Atkin, R. How Water Dissolves in Protic Ionic Liquids. *Angew. Chem., Int. Ed.* **2012,** *51*, 7468-7471.
48. Soper, A. K.; Howells, W. S.; Hannon, A. C. *ATLAS : Analysis of Time-of-Flight Diffraction Data from Liquid and Amorphous Samples*; Rutherford Appleton Laboratory: Didcot, 1989.
49. Soper, A. K. Empirical Potential Monte Carlo Simulation of Fluid Structure. *Chem. Phys.* **1996,** *202*, 295-306.
50. Soper, A. K. Partial Structure Factors from Disordered Materials Diffraction Data: an Approach Using Empirical Potential Structure Refinement. *Phys. Rev. B* **2005,** *72*, 104204.
51. Lopes, J. N. C.; Padua, A. A. H. Molecular Force Field for Ionic Liquids Composed of Triflate or Bistriflylimide Anions. *J. Phys. Chem. B* **2004,** *108*, 16893-16898.
52. Kashyap, H. K.; Hettige, J. J.; Annapureddy, H. V.; Margulis, C. J. Saxs Anti-Peaks Reveal the Length-Scales of Dual Positive-Negative and Polar-Apolar Ordering in Room-Temperature Ionic Liquids. *Chem. Commun.* **2012,** *48*, 5103-5.
53. Jan, N. Large Lattice Random Site Percolation. *Physica A* **1999,** *266*, 72-75.
54. Anouti, M.; Vigeant, A.; Jacquemin, J.; Brigouleix, C.; Lemordant, D. Volumetric Properties, Viscosity and Refractive Index of the Protic Ionic Liquid, Pyrrolidinium Octanoate, in Molecular Solvents. *J. Chem. Thermodyn.* **2010,** *42*, 834-845.
55. Amith, W. D.; Hettige, J. J.; Castner, E. W.; Margulis, C. J. Structures of Ionic Liquids Having Both Anionic and Cationic Octyl Tails: Lamellar Vacuum Interface vs Sponge-Like Bulk Order. *J. Phys. Chem. Lett.* **2016,** *7*, 3785-3790.
56. Shen, Y.; Kennedy, D. F.; Greaves, T. L.; Weerawardena, A.; Mulder, R. J.; Kirby, N.; Song, G. H.; Drummond, C. J. Protic Ionic Liquids with Fluorous Anions: Physicochemical Properties and Self-Assembly Nanostructure. *Phys. Chem. Chem. Phys.* **2012,** *14*, 7981-7992.
57. Hettige, J. J.; Araque, J. C.; Margulis, C. J. Bicontinuity and Multiple Length Scale Ordering in Triphilic Hydrogen-Bonding Ionic Liquids. *J. Phys. Chem. B* **2014,** *118*, 12706-12716.
58. Youngs, T. G. A. DLPUTILS: Calculate Properties from Molecular Dynamics Trajectories. https://www.projectaten.com/dlputils (accessed December 2016).
59. Headen, T. F.; Howard, C. A.; Skipper, N. T.; Wilkinson, M. A.; Bowron, D. T.; Soper, A. K. Structure of pi-pi Interactions in Aromatic Liquids. *J. Am. Chem. Soc.* **2010,** *132*, 5735-5742.
60. Matthews, R. P.; Welton, T.; Hunt, P. A. Competitive pi Interactions and Hydrogen Bonding within Imidazolium Ionic Liquids. *Phys. Chem. Chem. Phys.* **2014,** *16*, 3238-3253.
61. Hayes, R.; Imberti, S.; Warr, G. G.; Atkin, R. Effect of Cation Alkyl Chain Length and Anion Type on Protic Ionic Liquid Nanostructure. *J. Phys. Chem. C* **2014,** *118*, 13998-13998.
62. Israelachvili, J. N.; Mitchell, D. J.; Ninham, B. W. Theory of Self-Assembly of Hydrocarbon Amphiphiles into Micelles and Bilayers. *J. Chem. Soc., Faraday Trans. 2* **1976,** *72*, 1525-1568.

63. Israelachvili, J. N.; Marcelja, S.; Horn, R. G. Physical Principles of Membrane Organization. *Q. Rev. Biophys.* **1980,** *13*, 121-200.
64. Zemb, T. N.; Hyde, S. T.; Derian, P. J.; Barnes, I. S.; Ninham, B. W. Microstructure from X-Ray Scattering - the Disordered Open Connected Model of Microemulsions. *J. Phys. Chem.* **1987,** *91*, 3814-3820.
65. Strey, R. Microemulsion Microstructure and Interfacial Curvature. *Colloid Polym. Sci.* **1994,** *272*, 1005-1019.
66. Jiang, H. J.; FitzGerald, P. A.; Dolan, A.; Atkin, R.; Warr, G. G. Amphiphilic Self-Assembly of Alkanols in Protic Ionic Liquids. *J. Phys. Chem. B* **2014,** *118*, 9983-9990.
67. Murphy, T.; Hayes, R.; Imberti, S.; Warr, G. G.; Atkin, R. Ionic Liquid Nanostructure Enables Alcohol Self Assembly. *Phys. Chem. Chem. Phys.* **2016,** *18*, 12797-12809.

TOC Graphic